Ceramics International xxx (xxxx) xxx

Contents lists available at ScienceDirect

Ceramics International

journal homepage: www.elsevier.com/locate/ceramint

# Properties regulation of SiC ceramics prepared via stereolithography combined with reactive melt infiltration techniques

Wei Li [a,b], Congcong Cui [a,b,*], Jianxun Bao [a,b], Ge Zhang [a,b], Shan Li [c], Gong Wang [c]

[a] Changchun Institute of Optics, Fine Mechanics and Physics, Chinese Academy of Sciences, Changchun, 130033, China
[b] Key Laboratory of Optical System Advanced Manufacturing Technology, Chinese Academy of Sciences, Changchun, Jilin, 130033, China
[c] Technology and Engineering Center for Space Utilization, Chinese Academy of Sciences, Beijing, 100094, China

ARTICLE INFO

*Keywords:*
Stereolithography
Reactive melt infiltration
Impregnation method
Mechanical properties

ABSTRACT

Stereolithography(SLA) combined with reactive melt infiltration (RMI) is an effective way to fabricate silicon carbide(SiC) ceramic components with complex shapes and high precision. The purpose of this paper is to increase the content of SiC in the sintered body and improve the properties of SiC ceramics prepared by SLA/RMI technologies by the impregnation of the precursor of carbon source after debinding. The effects of the concentration of phenolic resin solution on the strength of sintered body were studied. The results show that this method can reduce the coefficient of thermal expansion and improve the thermal conductivity of the final body. At the same time, when the concentration of phenolic resin solution is 40 wt%, the final body obtained the best comprehensive properties. The value of bulk density, flexural strength and elastic modulus were 2.89 g/cm$^3$, 244.17 ± 5.13 MPa and 402.39 GPa, respectively. This strategy provides a promising prospect for the preparation of space optical mirrors with complex shapes and high strength by the SLA/RMI method.

## 1. Introduction

Reaction-bonded silicon carbide (RB-SiC) has the advantages of high stiffness, low density, good thermal dimensional stability, which makes it the most attractive candidate material for large-scale spatial optical mirrors [1]. To meet the needs of the application in space payloads, space mirrors are developed in the direction of lightweight and large aperture. This will require the mirror blank to have the optimum topological structure to ensure its overall structure stiffness and strength. So the structure of the mirror blank becomes more complicated [2,3]. Traditional manufacturing technologies mostly require the use of the mould with the designated shape [4–6]. However, once the shape of the mirror blank changes, the mould needs to be reprocessed, which inevitably increases the production cycle and manufacturing costs. Therefore, it is necessary to find an effective method to fabricate silicon carbide (SiC) ceramic optical mirrors with complex shape, high precision and excellent performance.

Additive manufacturing is a process in which 2D thin sheets with a specific shape are layered on the top of each other to form three-dimensional parts. It is a prospective process to overcome the problems faced by traditional manufacturing technology. At present, additive manufacturing technologies for ceramic components include laminated object manufacturing (LOM) [7], selective laser sintering (SLS) [8], direct ink writing (DIW) [9] and stereolithography (SLA) [10]. There are some defects to some extent, among SLS, LOM and DIW process, such as poor surface quality, low forming accuracy and efficiency, which will be difficult to meet the needs of SiC lightweight structure with high strength and stiffness. Due to the advantages of high forming accuracy and uniform composition, SLA is expected to produce complex ceramic components.

At present, there have been some researches on SiC ceramics prepared by the SLA/RMI method. Tian [11] successfully prepared RB-SiC by SLA/RMI method, but the flexural strength of the RB-SiC was 127.8 MPa; In order to improve the mechanical properties of RB-SiC, Heng Zhang [10] prepared the photosensitive suspension including chopped carbon fibers, the SiC green body was successfully prepared, and the maximum flexural strength reached 262.2 MPa after RMI. However, the introduction of carbon fibers increases the cost.

Recently, Zou [12] fabricated RB-SiC by SLS combined with RMI and studied the effect of preform impregnation with phenolic(PF) resin solution on the properties of the final RB-SiC. The flexural strength of the specimens impregnated with PF resin was 7% higher than that of the specimens without impregnation. The impregnation treatment is an economical and effective way to improve the comprehensive

* Corresponding author. Changchun Institute of Optics, Fine Mechanics and Physics, Chinese Academy of Sciences, Changchun, 130033, China.
*E-mail address:* cuicongconghit@126.com (C. Cui).

https://doi.org/10.1016/j.ceramint.2021.08.307
Received 22 May 2021; Received in revised form 24 August 2021; Accepted 25 August 2021
Available online 26 August 2021

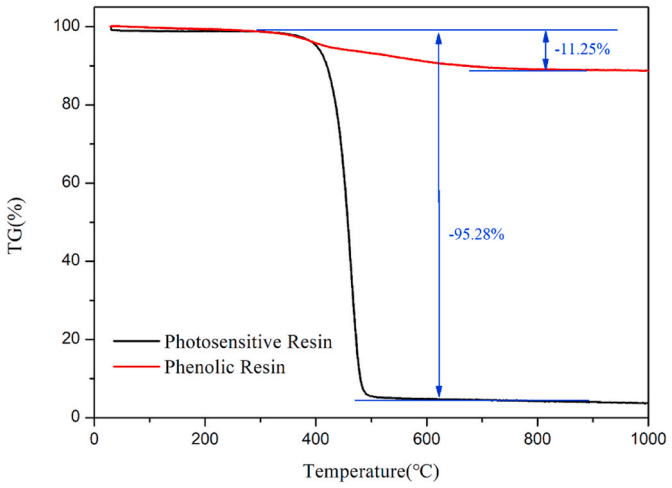


**Fig. 1.** The thermogravimetric(TG) analysis curves of photosensitive resin and PF resin.

performance of RB-SiC prepared by SLA/RMI method. However, the method for preform impregnation with PF resin has hardly been reported in RB-SiC ceramics prepared by SLA combined with RMI. Therefore, in this study, SiC green body was prepared by SLA, after pyrolysis, the SiC green body was impregnated with PF resin solution, the PF resin could be decomposed into pyrolytic carbon under high temperature conditions, so as to increase the carbon content in the green body, and then the SiC content in the sintered body was increased via RMI process, and finally the comprehensive performance of the material was improved.

In this study, the effects of the concentration of PF resin solution on the bulk density, elastic modulus, flexural strength, linear expansion coefficient and thermal conductivity of RB-SiC at room temperature were studied.

## 2. Experimental

### 2.1. Materials

The main raw materials include phenolic(PF) resin (665, Changchun Shengda Insulation Material Co., Ltd, China), ethyl alcohol (Analytical Reagent, Beijing Institute of Chemical Reagents) as a solvent for PF resin and commercial micron-sized α-SiC (purity≥99.5%, d50 = 54.77 μm). For the 3D printing process, the photosensitive resin (UV-3050, Dong-Guan Inoue new material development Co., Ltd, China) and the photoinitiator (TPO; purity: 97%; Shanghai Aladdin Biochemical Technology Co., Ltd., China) which is sensitive to the 405 nm wavelength UV light are also required. The thermogravimetric(TG) analysis curves of photosensitive resin and PF resin are shown in Fig. 1. In addition, commercial silicon powders (purity = 99%, d50 = 5 μm) are placed on the specimen during infiltration and the β-SiC (purity ≥99%, d50 = 50 nm) was used as a reference in XRD results.

### 2.2. Fabrication of RB-SiC

Here, RB-SiC was prepared by Stereolithography (SLA) and reactive melt infiltration (RMI).

#### 2.2.1. The preparation of silicon carbide green body by SLA

First, the silicon carbide powders with the ratio of 47 vol%, photosensitive resin and photoinitiator were mixed in the ball mill machine for 5 h, and the homogeneous photocurable slurry was synthesized. Then, the 3D STL model of the silicon carbide ceramic mirror was designed by computer and imported into the 3D printer (CeraStation 160, Jiangsu qiandugaoke Co., Ltd), as shown in Fig. 2. Finally, the green body was prepared by SLA, and the wavelength of UV light, light intensity, exposure time and the thickness of each layer were 405 nm, 90μw/cm$^2$, 1.9s and 50 μm, respectively.

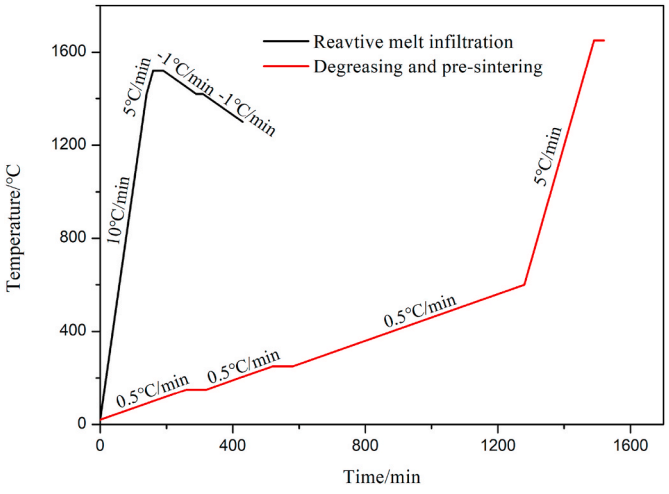


**Fig. 3.** The fabricated schematic of RB-SiC parts including: preform impregnation and RMI.

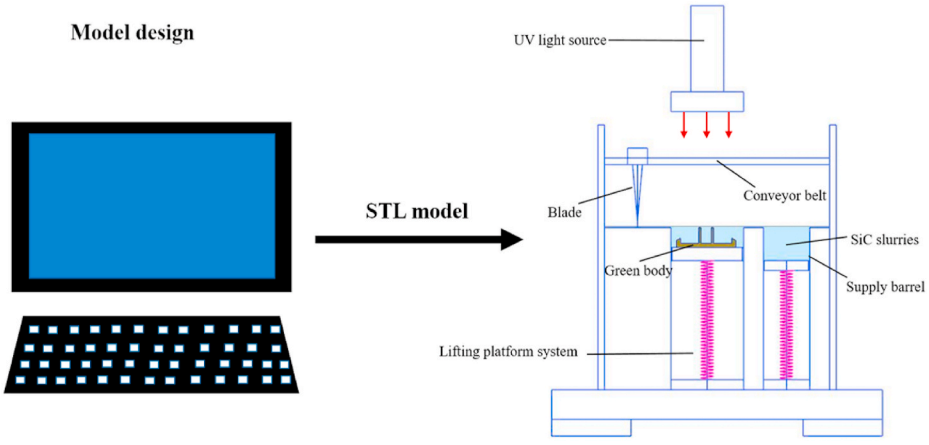


**Fig. 2.** Flow diagram of preparing silicon carbide green body by SLA. (For interpretation of the references to colour in this figure legend, the reader is referred to the Web version of this article.)

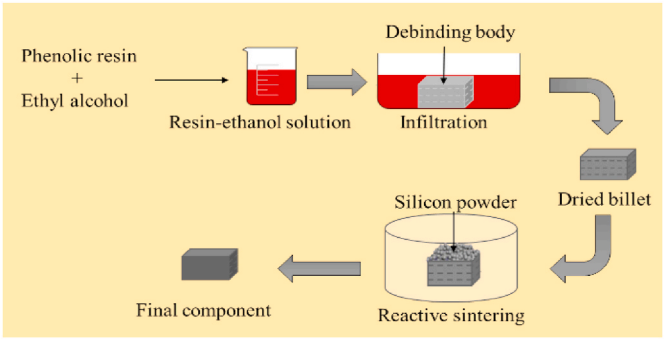


**Fig. 4.** The heating program for debinding and RMI.

### 2.2.2. The post-treatment technology of silicon carbide green body

The heating program of the debinding process is shown in Fig. 3, which was set based on the properties of photosensitive resin. The heating rate before 650 °C did not exceed 0.5 °C/min, and the temperature was kept at 450 °C for 30 min, to ensure that the gas produced by organics slowly escaped from the green body during debinding. Subsequently, the specimens were rapidly heated to 1650 °C for pre-sintering to guarantee the mechanical strength required during the post processing [13]. Then, the specimens were classified into three groups. The specimens of each group were impregnated with different concentrations of the resin-ethanol solution with the resin content of 30 wt%, 40 wt% and 50 wt%, respectively. The impregnated specimens were dried in an oven at 100 °C for 10 h and then cured at 180 °C for 2 h. After curing, these specimens were pyrolyzed and pre-sintered in a chamber furnace in a vacuum at 1650 °C for 0.5 h. Finally, RB-SiC was obtained after liquid melt silicon infiltration of the three groups of specimens, named S30, S40 and S50 corresponding to the resin-ethanol solution concentration of 30 wt%, 40 wt% and 50 wt%, respectively. In addition, a standard group named S0, which was not impregnated with resin-ethanol solution, was carried out with the same process and compared with S30, S40 and S50. Fig. 4 shows the fabrication process of RB-SiC, including perform impregnation and reactive melt infiltration (RMI).

The RMI process was as follows: First, the silicon powders were evenly distributed on the upper surface of the specimens. Then, the specimens were then heated to 1520 °C for 30 min using a chamber furnace under the vacuum condition until the end of the experiment, and the program is shown in Fig. 3. Finally, after cooling to room temperature, all specimens were taken out and subjected to materials characterization and performance tests.

### 2.3. Testing and characterization

A scanning electron microscopy (SEM, Phenom ProX, Netherlands) and an optical microscope(OLYMPUS-BX51 M) were employed to observe the microstructures. The bulk density and apparent porosity of the RB-SiC composites were determined based on the Archimedes' principle. The phase composition was analyzed by XRD (Bruker/D8 FOCUS, German), with a Cu Kα radiation source. Raman measurements were conducted on a confocal Raman microspectrometer (HOOKE P300, HOOKE Instruments Ltd., China) equipped with a 532 nm solid-state laser and a −70 °C cooled CCD detector. The laser beam was focused by a 100x objective (0.85 NA) which provides a lateral resolution of <1 μm. For a single spectrum, the power at the specimen was 10 mW and the exposure time equaled to 2 s with a spectral resolution < 2 $cm^{-1}$. The main spectral regions in this study are as follows [14]:

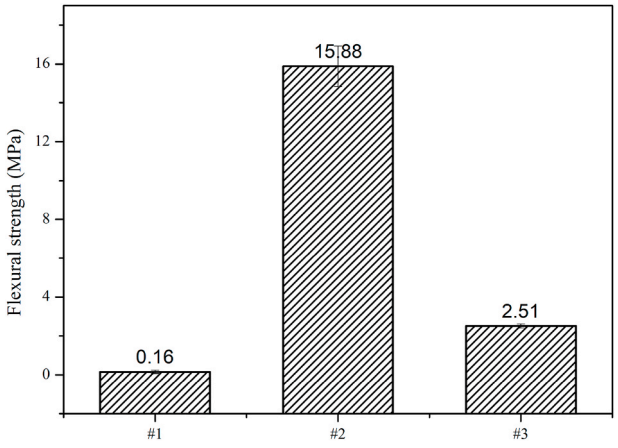


**Fig. 6.** Flexural strength of the specimens in each stage before RMI: #1 after pyrolysis; #2 after curing; #3 after debinding.

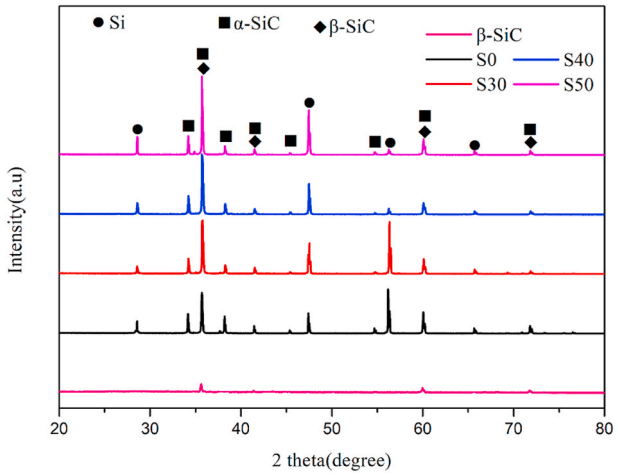


**Fig. 7.** XRD pattern of sintered specimens and β-SiC.

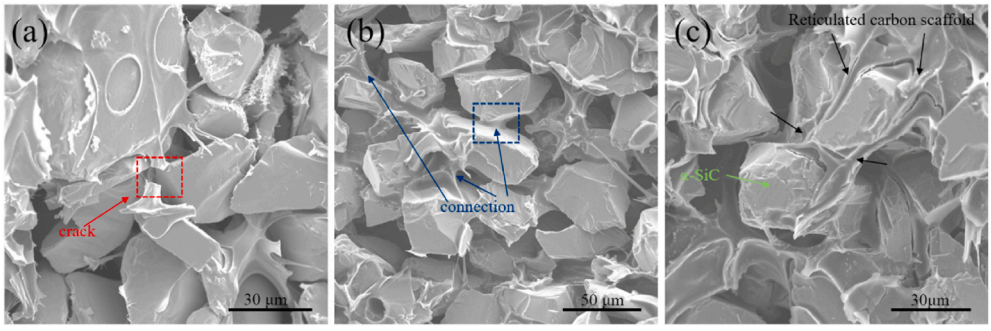


**Fig. 5.** Microstructure of the specimens in each stage before RMI: (a) #1 after pyrolysis; (b) #2 after curing; (c) #3 after debinding.

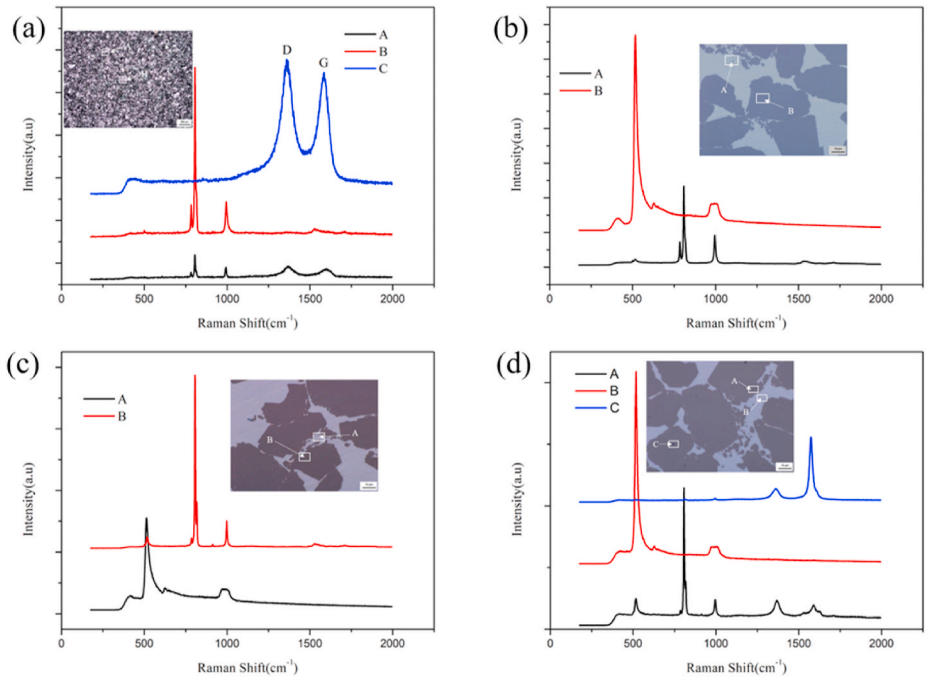


**Fig. 8.** Raman analysis of (a) #3, (b) S30, (c) S40 and (d) S50.

**Table 1**
Intensities and wave numbers(cm$^{-1}$) corresponding to D and G bands of the Raman spectra of specimen #3 and S50 in Fig. 6.

| Specimen | Band | Max. Intensity(a.u) | Wave number(cm$^{-1}$) |
|---|---|---|---|
| #3 | D | 3778 | 1358.52 |
| | G | 3465 | 1585.35 |
| S50 | D | 2781 | 1361.08 |
| | G | 11169 | 1573.58 |

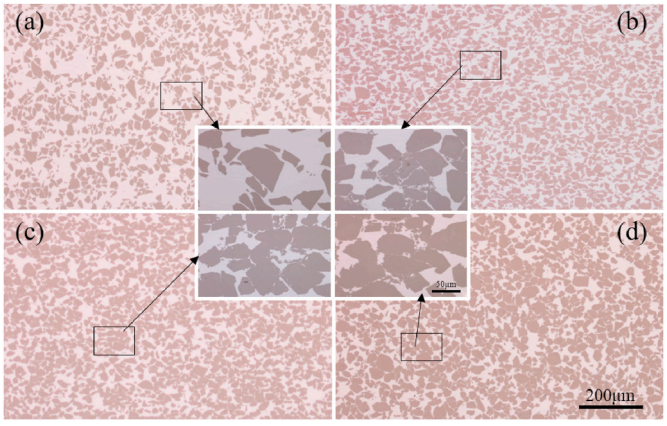


**Fig. 9.** Morphology of the polished surface of RB-SiC for (a) S0, (b) S30, (c) S40 and (d) S50.

(1) the characteristic peak at 520 cm$^{-1}$ corresponds to crystallized silicon.
(2) the characteristic peak at 790 cm$^{-1}$ and 960 cm$^{-1}$ corresponds to silicon carbide.
(3) the characteristic peak at 1350 cm$^{-1}$(D peak) and 1590 cm$^{-1}$(G peak) correspond to carbon.

In terms of thermal dimensional stability, the linear expansion coefficient(CTE) was measured by linear dilatometer (DIL 402C, NETZSCH, German) over the temperature range 0 °C–100 °C; The thermal diffusivity of the specimens was measured by LFA467Hyper Flash (NETZSCH, German) from −30 °C to 20 °C, and the specific heat capacity of the specimens from −30 °C to 20 °C under Argon atmosphere were measured by differential scanning calorimetry (DSC200F3, NETZSCH, German). The thermal conductivity (λ) of RB-SiC was calculated by Eq.(l) [15]:

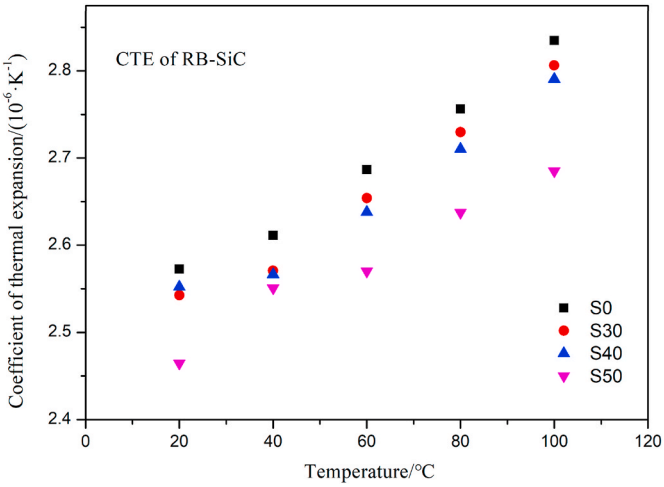


**Fig. 10.** The coefficient of thermal expansion from 0 °C to each temperature range for S0, S30, S40 and S50.

$$\lambda = \alpha \cdot \rho \cdot c_p \quad (1)$$

where α is the thermal diffusivity, ρ is the bulk density, and $c_p$ is the specific heat capacity of the specimens.

The mechanical strength of the specimens was carried out by three-point bending method by a universal testing machine (Instron 1195, USA) according to the Chinese Testing Standard GB/T 4741–1999. The span and loading rate are 30 mm and 0.5 mm/min, respectively, and the

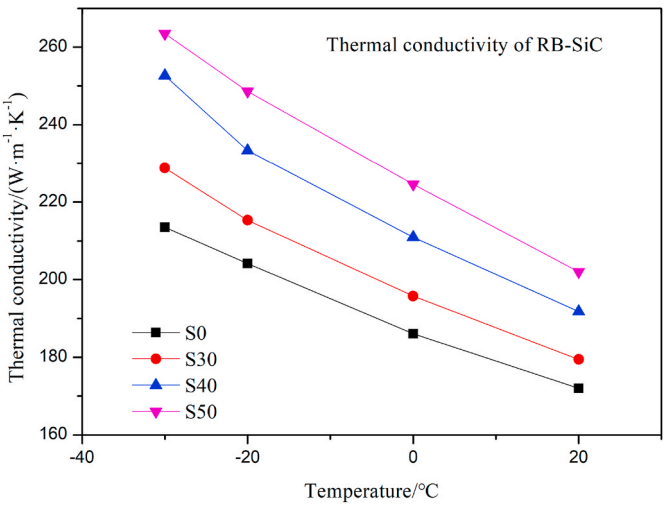


**Fig. 11.** The thermal conductivity of S0, S30, S40 and S50 as function of temperature (Solid line is empirical formula fitting to data).

**Table 2**
Thermodynamic properties of SiC ceramics prepared by different processes at room temperature.

| Fabrication process | CTE(1 × $10^{-6}$/K) | Thermal conductivity (W/m·K) | Ref. |
|---|---|---|---|
| Gel-casting + RMI | 3.4 | 161 | [25] |
| Pressureless sintering | – | 73 | [26] |
| Spark plasma sintering | – | 104 | [27] |
| Tape casting + pressureless sintering | 3.7(300 °C) | 138 | [28] |
| SLA + RMI | 2.46–2.54 | 179.44–202.04 | This work |

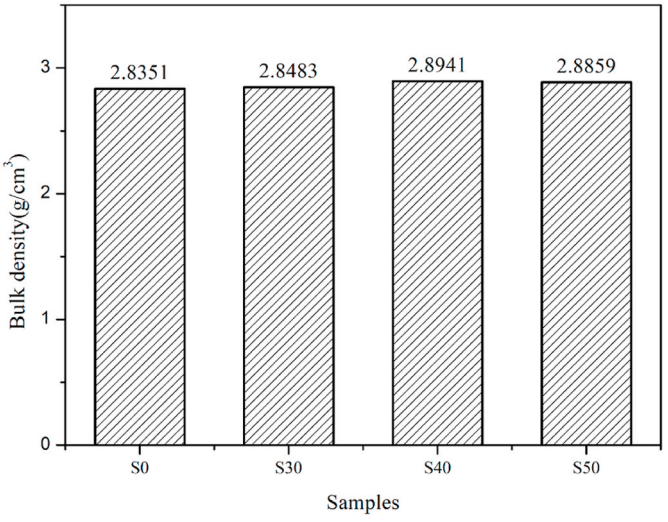


**Fig. 12.** The bulk density of RB-SiC for S30, S40 and S50.

loading direction was consistent with the SLA forming direction. The dimensions of specimens in flexural strength testing were around 3 mm × 4 mm × 36 mm. Seven specimens of each group were tested; the mean value and the standard deviation were calculated from the results.

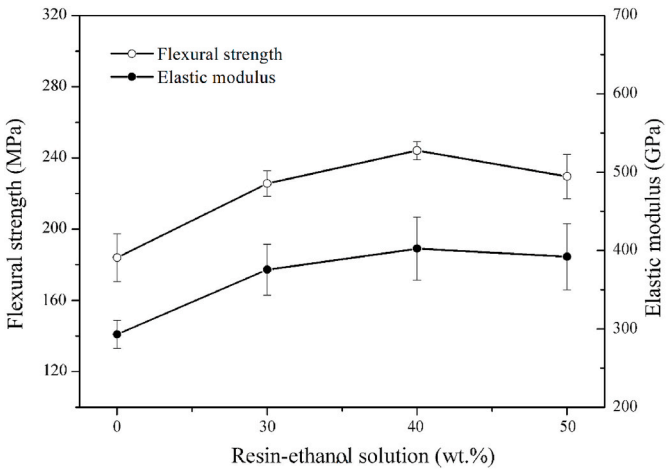


**Fig. 13.** Flexural strength and elastic modulus of S0, S30, S40 and S50.

**Table 3**
Comparison of different methods to improve the flexural strength of RB-SiC prepared by SLA with RMI.

| 3D printed ceramics | Fabrication process | Method | Flexural strength | Ref. |
|---|---|---|---|---|
| SiC | SLA + RMI | The PF resin was added to the photosensitive resin to increase the carbon content in the green body | 127.8 ± 0.5 MPa | [11] |
| Cf/SiC | DLP + RMI | The chopped carbon fibers were added to the photosensitive resin | 262.6 MPa | [10] |
| SiC | SLA + RMI | The RB-SiC was prepared by SLA combined with RMI. | 210.4 ± 10.3 MPa | [29] |
| SiC | SLA + RMI | Resin-ethanol was impregnated as a precursor of carbon source | 244.17 ± 5.13 MPa | This work |

## 3. Results and analysis

### 3.1. Microstructure and mechanical properties after carbonization

#### 3.1.1. Microstructure before reactive melt infiltration (RMI)

In order to obtain SiC ceramics, the polymers such as photosensitive resins, photoinitiators, etc., must be burnt out from the green body. Fig. 5 shows the microstructure of the green body prepared by SLA in each stage before RMI, such as the specimen was pyrolyzed at 650 °C (named #1), the #1 was impregnation with PF resin solution for curing (named #2), and the #2 was debinded and pre-sintered (named #3). As shown in Fig. 1, due to the carbon residual rate of the photosensitive resin after pyrolysis at 650 °C was less than 5 wt%, there are few connections among α-SiC particles in Fig. 5(a). Fig. 5(b) shows that after the impregnation of PF resin, the α-SiC particles were tightly connected by the pyrolytic carbon and the PF resin after curing. #3 shows that pyrolytic carbon distributed uniformly in the green body with a network structure in Fig. 5(c), which acted as a connection among SiC particles. The reticulated carbon scaffold increased the strength of the body after carbonization as well as plays a role in fixing the position of SiC particles to prevent collapse or warping after pyrolysis.

#### 3.1.2. Mechanical properties before reactive melt infiltration (RMI)

The flexural strength of #1, #2 and #3 was measured by three-point bending method. The results are shown in Fig. 6. Compared with #1, the flexural strength of #2 was greatly improved, indicating that the PF resin solution was successfully impregnated into the green body, and the PF resin reinforced the green body significantly after curing. During

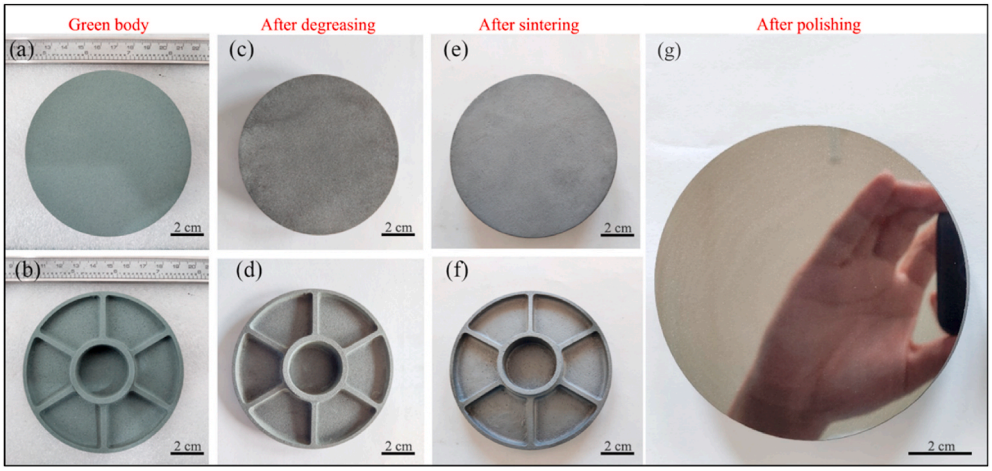


**Fig. 14.** Photos of lightweight SiC spatial optical mirror: (a, b) the green body prepared by SLA; (c, d) after debinding; (e, f) after RMI; (g, h) after polishing.

curing, phenolic resin formed a reticulated polymeric scaffold among the SiC particles, following the evaporation of anhydrous ethanol. After carbonization, the phenolic resin was transformed into pyrolytic carbon. Compared with #1, the flexural strength of #3 is greatly improved, that is to say, impregnating resin-ethanol solution can effectively increase the content of pyrolytic carbon in the green body [16]. Besides, the pyrolytic carbon played a role in the connection among the SiC particles.

### 3.2. Microstructure and properties of RB-SiC

Generally speaking, the mechanical properties of ceramic materials depend on their microstructure, which largely depends on the composition of the green body before reactive melt infiltration (RMI). At present, the introduction of pyrolytic carbon into the green body before RMI is one of the effective means to improve the properties of SiC ceramic materials.

#### 3.2.1. Phase analysis of sintered specimens

Fig. 7 exhibits the XRD results of sintered specimens and β-SiC powders. The results show that no residual carbon was detected in the sintered body after RMI. The sintered body consists of α-SiC, β-SiC and silicon. The α-SiC was the raw material powder in the 3D printing process, and β-SiC was formed during the reaction sintering process [12, 17]. At the same time, β-SiC could be observed in S0 in Fig. 7, which was caused by the pyrolysis carbon left in the green body after the pyrolysis of photosensitive resin, dispersants and other organics. This part of pyrolysis carbon also provided the carbon source for the reaction sintering process.

#### 3.2.2. Raman analysis of #3, S30, S40 and S50

The Raman spectroscopy was performed to observe whether there was residual carbon in the near-surface regions. Fig. 8 shows the Raman spectroscopic analysis of different visual appearances (bright and dark zones) in the optical image of the specimens. In Fig. 8(a) and (d), both D and G bands exist in #3 and S50, and the intensities and wave numbers ($cm^{-1}$) corresponding to D and G bands of the Raman spectra of specimen #3 and S50 are shown in Table 1. As known from the calculation, the ratio of $I_D/I_G$ is higher for #3 compared with S50 (1.09 and 0.25 respectively). The ratio of $I_D/I_G$ is related to the crystallinity of carbon, A. Inam [18] reported that the radios of $I_D/I_G$ range from 0.1 to 0.3 and 1 to 2.6 for the carbon with highly and poor crystallinity. Therefore, the residual carbon that existed in S50 was transformed into the graphite phase embedded in the dark zones as shown in Fig. 8(d). As shown in Fig. 8(b) and (c), the absence of D and G bands indicates that the pyrolytic carbon had been totally reacted. Only silicon and silicon carbide existed in S30 and S40, which is consistent with the results of XRD.

#### 3.2.3. Microstructure of RB-SiC

During the reactive melt infiltration process, the molten silicon contacted with the carbon in the green body, and β-SiC is formed [12, 17]. When the pyrolytic carbon inside the green body is completely reacted, the remaining pores are filled with molten silicon and the densification of the material is finally realized.

After grinding and polishing, the microstructures of the sintered specimens are shown in Fig. 9. The RB-SiC composite was composed of SiC (α-SiC and β-SiC) as the dark grey and silicon as the bright. As the PF resin concentration increased, the area of dark grey increased from Fig. 9(a)–9(d), this indicates that the content of SiC in the composites increased. In the meantime, the pyrolytic carbon had been reacted and SiC was synthesized in situ. Compared with S0, more SiC particles were observed in S30, S40 and S50, which would reduce the size and content of silicon and facilitate the improvement of performance.

#### 3.2.4. Thermal properties of RB-SiC

From the viewpoint of the thermodynamic properties, thermal dimensional stability is an important factor to ensure the stable focal length and image quality. The main thermal properties determining the thermal dimensional stability are the linear expansion coefficient(CTE) and the thermal conductivity [19]. Fig. 10 shows the measured results of the CTE for each specimen. The CTE is subjected to variations as the temperature changes, often increasing as the temperature increases, which resembles most polycrystalline materials [20,21]. Normally, the CTE of ceramic materials is the result of several factors, such as the composition of the material, the content and distribution of the reinforcing phase, and the defects generated during the preparation process [22]. According to the measurement results of Marshall et al. [23], the CTE of SiC is lower than that of silicon ($2.3 \times 10^{-6}$ $K^{-1}$ and $2.6 \times 10^{-6}$ $K^{-1}$ respectively at room temperature). Therefore, by impregnating resin-ethanol solution, the coefficient of thermal expansion of RB-SiC decreases significantly and the RB-SiC prepared by this method has better dimensional stability.

The thermal diffusivity(α) and specific heat capacity($c_p$) were measured at different temperatures, substituting α, $c_p$ and relative density of each specimen into Formula (1), respectively, the thermal conductivity was obtained as shown in Fig. 11, the solid line represents the fitting of two adjacent data. Different from the free electron heat transfer in metals, the heat transfer in ceramics depends on phonons. The thermal conductivity varies with the changes of temperature and decreases as the temperature increases [20,24]. Comparing S0 with S30, S40 and S50, it can be found that the method of impregnation resin-ethanol solution can improve the thermal conductivity of the materials. The increase of the thermal conductivity from S0 to S50 is due to the increase in the content of SiC. According to Marshall's report, the

thermal conductivity of SiC is higher than that of silicon [23]. In addition, the residual graphite in S50 is conducive to the improvement of thermal conductivity. S30, S40 and S50 all have low thermal expansion coefficients and high thermal conductivity, which makes the RB-SiC obtain better thermal stability, and the temperature gradient of the mirrors is reduced.

For space optical mirrors, low linear expansion coefficient and high thermal conductivity are the keys to ensure the stability of the focal length and image quality. The thermal dimensional stability of SiC ceramics prepared by different techniques at room temperature is shown in Table 2. According to Table 2, the thermodynamic dimensional stability of SiC ceramics prepared by this method is better than those of other traditional manufacturing methods. Therefore, according to the test results, it is indicated that it is highly feasible to impregnate PF resin solution before RMI to improve the properties of SiC ceramics.

#### 3.2.5. The bulk density and strength of RB-SiC

In this study, RB-SiC was fabricated by the infiltration of porous C/SiC preform with liquid silicon, and the porous carbon was formed after the pyrolysis of phenolic resin as the carbon source. The porous carbon inter-connected pores provided the necessary channels for the infiltration of molten silicon into the preform, which can effectively avoid the phenomenon of infiltration blocking. The measurement of apparent porosity can be used to verify whether there is the phenomenon of infiltration blocking to some extent. The apparent porosity of S0, S30, S40 and S50 are 0.0253%, 0.0163%, 0.0124% and 0.1162%, respectively, which indicated that the sintering process was reasonable and the phenomenon of infiltration blocking hardly existed. Fig. 12 shows the bulk density of S0, S30, S40 and S50 (The standard deviations of measuring the bulk density of S0, S30, S40 and S50 are 0.0058, 0.0012, 0.0064 and 0.0002. Therefore, the error bar is too small to be shown in Fig. 12). Since the density of silicon carbide and silicon at room temperature are 3.21 g/cm$^3$ and 2.34 g/cm$^3$, the content of silicon carbide is positively correlated with the bulk density of RB-SiC composites. Compared with S0 and S30, it can be found that the density of S30 is higher, indicating that the impregnation method can effectively increase the content of SiC in the RB-SiC composites. When the resin content increased, the pyrolytic carbon introduced into the green body increased, which results in the increase of SiC content and decrease of free silicon content in RB-SiC composites. However, when the resin content increased to 50%, its bulk density decreases slightly. According to the Raman spectrum analysis in Fig. 8, this is due to the presence of graphite in S50.

The mechanical properties of RB-SiC composites fabricated by SLA and RMI are shown in Fig. 13. Via impregnation, the properties of sintered body were improved significantly. By the impregnation of carbon precursor solution, the carbon source was successfully introduced into the green body. After RMI, the content of SiC in RB-SiC composites increased and the content of free silicon decreased. Compared S0 with S30, the flexural strength of RB-SiC increased from 184.01 $\pm$ 13.48 MPa to 225.61 $\pm$ 7.12 MPa after impregnation with the resin-ethanol solution. Further increasing the concentration of resin solution, the flexural strength of RB-SiC reached the maximum value, which is 244.17 $\pm$ 5.13 MPa. At the same time, the elastic modulus also tended to the maximum value, which was 402.39 $\pm$ 40.12 GPa, and the resin-ethanol solution concentration reached the best value. As for S50, the flexural strength and elastic modulus decreased.

The main reason is that the residual graphite in S50 as the impurities, which lead to the decline of the mechanical properties. The mechanical properties of materials are not only related to the composition and structure, but also related to the defects of the materials. The residual graphite is easy to peel off during grinding and polishing. This will leave pores in the materials, which can also lead to a decrease in the mechanical properties of the materials. Table 3 lists the results of other reported methods to improve the properties of RB-SiC composites fabricated by SLA with RMI. When Tian [11] added PF into the photosensitive resin solution, the flexural strength of RB-SiC was not obviously improved. In this work, the preform was used to impregnate PF solution, which was similar to Zhang's [10] result of using carbon fiber as reinforcement. However, the PF resin was more cost-saving than the carbon fiber. We can conclude that impregnation resin-ethanol solution is one of the most effective methods at present.

For the application of space mirror, RB-SiC must have high specific stiffness to avoid the deflection under self-load. S40 not only has the highest specific stiffness, but also has the properties of high flexural strength, low CTE and high thermal conductivity. Therefore, S40 is more suitable for space mirror materials. As shown in Fig. 14, the lightweight SiC spatial optical mirror was successfully prepared by the method above. Firstly, the green body was prepared by SLA method, as shown in Fig. 14(a) and (b). After debinding, no obvious cracks, pores and other defects were observed, and the integrity of the green body is great, as shown in Fig. 14(c) and (d). The green body was impregnated with 40 wt % PF resin solution to improve its comprehensive properties. After curing and debinding, the SiC spatial optical mirror was completely densified by RMI, as shown in Fig. 14(e) and (f). Finally, after polishing, Fig. 14(g) shows that the SiC spatial optical mirror exhibited high quality and optical properties.

## 4. Conclusion

Preform impregnation can optimize the microstructure of RB-SiC composites prepared by stereolithography(SLA) and reactive melt infiltration (RMI), and the thermal dimensional stability and mechanical properties of RB-SiC can be enhanced. As the carbon precursor, phenolic resin and anhydrous ethanol are prepared to be impregnated into the green body, and after high-temperature carbonization, the reticulated carbon scaffold was left in the green body, which played a role in connection among the SiC particles in the green body after carbonization. Secondary β-SiC was synthesized in situ by reaction of molten silicon and pyrolytic carbon after reactive melt infiltration. This method enables RB-SiC composites to have better thermal dimensional stability and higher strength. When the concentration of impregnation resin-ethanol solution is 40 wt%(S40), the comprehensive properties of the final RB-SiC are the best compared with concentration of 30 wt% (S30) and 50 wt%(S50).

## Declaration of competing interest

The authors declare that they have no known competing financial interests or personal relationships that could have appeared to influence the work reported in this paper.

## Acknowledgements

This research did not receive any specific grant from funding agencies in the public, commercial, or not-for-profit sectors.

## References

[1] G. Liu, X. Zhang, J. Yang, G. Qiao, Recent advances in joining of SiC-based materials (monolithic SiC and $SiC_f$/SiC composites): joining processes, joint strength, and interfacial behavior, J. Journal of Advanced Ceramics 8 (2019) 19–38, https://doi.org/10.1007/s40145-018-0297-x.

[2] S. Guo, G. Zhang, L. Li, W. Wang, X. Zhao, Effect of materials and modelling on the design of the space-based lightweight mirror, J. Mater. Des. 30 (2009) 9–14, https://doi.org/10.1016/j.matdes.2008.04.056.

[3] H. Kihm, H.S. Yang, Design optimization of a 1-m lightweight mirror for a space telescope, J. Opt. Eng. 52 (2013), 091806, https://doi.org/10.1117/1.OE.52.9.091806.

[4] Kai Liu, Tian Wu, David L. Bourell, et al., Laser additive manufacturing and homogeneous densification of complicated shape SiC ceramic parts, J. Ceramics Int. 44 (2018) 21067–21075, https://doi.org/10.1016/j.ceramint.2018.08.143.

[5] Shuang Li, Yumin Zhang, Jiecai Han, et al., Effect of carbon particle and carbon fiber on the microstructure and mechanical properties of short fiber reinforced reaction bonded silicon carbide composite, J. Eur. Ceram. Soc. 33 (4) (2013) 887–896, https://doi.org/10.1016/j.jeurceramsoc.2012.10.026.

[6] Wenhu Hong, Ping Hu, Dongyang Zhang, et al., Fabrication of ZrB 2 -SiC ceramic composites by optimized gel-casting method, J. Ceram. Int. 44 (2018) 6037–6043, https://doi.org/10.1016/j.ceramint.2017.12.227.
[7] Shichao Liu, Feng Ye, Limeng Liu, et al., Feasibility of preparing of silicon nitride ceramics components by aqueous tape casting in combination with laminated object manufacturing, J. Mater. Des. 66 (2015) 331–335, https://doi.org/10.1016/j.matdes.2014.10.079.
[8] Annan Chen, Jiamin Wu, Kai Liu, et al., High-performance ceramic parts with complex shape prepared by selective laser sintering: a review, J. Adv. Appl. Ceram. 117 (2018) 100–117, https://doi.org/10.1080/17436753.2017.1379586.
[9] Heng Zhang, Yong Yang, Bin Liu, et al., The preparation of SiC-based ceramics by one novel strategy combined 3D printing technology and liquid silicon infiltration process, Ceram. Int. 45 (8) (2019) 10800–10804, https://doi.org/10.1016/j.ceramint.2019.02.154.
[10] Heng Zhang, Yong Yang, Kehui Hu, et al., Stereolithography-based additive manufacturing of lightweight and high-strength Cf/SiC ceramics, J. Addit. Manuf. 34 (2020) 101199, https://doi.org/10.1016/j.addma.2020.101199.
[11] Xiaoyong Tian, Weigang Zhang, Dichen Li, et al., Reaction-bonded SiC derived from resin precursors by Stereolithography, J. Ceramics Int. 38 (2012) 589–597, https://doi.org/10.1016/j.ceramint.2011.07.047.
[12] Yang Zou, Chen Hui Li, Yihao Tang, et al., Preform impregnation to optimize the properties and microstructure of RB-SiC prepared with laser sintering and reactive melt infiltration, J. Eur. Ceram. Soc. 40 (2020) 5186–5195, https://doi.org/10.1016/j.jeurceramsoc.2020.07.023.
[13] Shu Cao, Fangxia Xie, Xueming He, et al., Postprocessing study for the controllable structures of ceramic green parts realized by a flexible binder jetting printing(BJP) solution, J. Adv. Mater. Sci. Eng., https://doi.org/10.1155/2020/3865752.
[14] Elisa Padovano, Mauro Giorcelli, Giovanni Bianchi, et al., Graphite-Si-SiC ceramics produced by microwave assisted reactive melt infiltration, J. Eur. Ceram. Soc. 39 (2019) 2232–2243, https://doi.org/10.1016/j.jeurceramsoc.2019.01.057.
[15] Yao Wang, Yumin Zhang, Jiecai Han, et al., Fabrication and test of reaction bond silicon carbide for optical applications, J. Trans. Nonferrous Metals Soc. China 16 (2006) 409–413, https://doi.org/10.1016/S1003-6326(06)60070-8.
[16] Xiaohong Xia, Hongbo Liu, Yuede He, et al., Investigation of porous carbon fabricated by polymer blending of phenolic resin and suberic acid, J. Iran. Chem. Soc. 9 (2012) 545–550, https://doi.org/10.1007/s13738-012-0067-6.
[17] Xuejian Bai, Guojiao Ding, Keqiang Zhang, et al., Stereolithography additive manufacturing and sintering approaches of SiC ceramics, J. Open Ceram. 5 (2021) 100046, https://doi.org/10.1016/j.oceram.2020.100046.
[18] A. Inam, R. Brydson, D.V. Edmonds, Raman spectroscopy study of the crystallinity of graphite formed in an experimental free-machining steel, J. Mater. Char. 163 (2020) 110264, https://doi.org/10.1016/j.matchar.2020.110264.
[19] Balanand Santhosh, Emanuel Ionescu, Francesco Andreolli, et al., Effect of pyrolysis temperature on the microstructure and thermal conductivity of polymer-derived monolithic and porous SiC ceramics, J. Eur. Ceram. Soc. 41 (2021) 1151–1162, https://doi.org/10.1016/j.jeurceramsoc.2020.09.028.
[20] Hua Fu, Wei Zhu, Zhongfeng Xu, et al., Effect of silicon addition on the microstructure, mechanical and thermal properties of C f/SiC composite prepared via selective laser sintering, J. Alloys Compd. 792 (2019) 1045–1053, https://doi.org/10.1016/j.jallcom.2019.04.129.
[21] A. Michaux, C. Sauder, G. Camus, et al., Young's modulus, thermal expansion coefficient and fracture behavior of selected Si–B–C based carbides in the 20–1200°C temperature range as derived from the behavior of carbon fiber reinforced microcomposites, J. Eur. Ceram. Soc. 27 (2007) 3551–3560, https://doi.org/10.1016/j.jeurceramsoc.2006.12.006.
[22] Reza Zare, Sharifi Hassan, Mohammad Reza Saeri, et al., Investigating the effect of SiC particles on the physical and thermal properties of Al6061/SiCp composite, J. Alloys Compd. 801 (2019) 520e528, https://doi.org/10.1016/j.jallcom.2019.05.317.
[23] A.L. Marshall, P. Chhillar, P. Karandikar, et al., The effects of Si content and SiC polytype on the microstructure and properties of RBSC, in: J. Salem, G. Hilmas, W. Fahrenholtz (Eds.), Mechanical Properties and Processing of Ceramic Binary, Ternary, and Composite Systems, John Wiley & Sons, Hoboken, 2009, pp. 115–126, https://doi.org/10.1002/9780470456361.ch12.
[24] Yuying Zhang, Tianshi Wang, Chun-Yen Hsu, et al., Thermal transport characteristics in diamond/SiC composites via molten Si infiltration, J. Ceramics Int. 47 (2021) 17084–17091, https://doi.org/10.1016/j.ceramint.2021.03.017.
[25] Yumin Zhang, Jianhan Zhang, Jiecai Han, et al., Large-scale fabrication of lightweight Si/SiC ceramic composite optical mirror, J. Mater. Lett. 58 (2004) 1204–1208, https://doi.org/10.1016/j.matlet.2003.09.010.
[26] Valmikanathan P. Onbattuvelli, Ravi K. Enneti, Sundar V. Atre, The effects of nanoparticle addition on the densification and properties of SiC, J. Ceram. Int. 38 (2012) 5393–5399, https://doi.org/10.1016/j.ceramint.2012.03.049.
[27] Zhenfei Chai, Zhaohe Gao, Liu Han, et al., Thermal conductivity of spark plasma sintered SiC ceramics with Alumina and Yttria, J. Eur. Ceram. Soc. 41 (2021) 3264–3273, https://doi.org/10.1016/j.jeurceramsoc.2020.12.020.
[28] W.S. Yang, S. Biamino, E. Padovano, et al., Thermophysical properties of SiC multilayer prepared by tape casting and pressureless sintering, J. Composite Struct. 96 (2013) 469–475, https://doi.org/10.1016/j.compstruct.2012.09.018.
[29] Xuejian Bai, Guojiao Ding, Keqiang Zhang, et al., Stereolithography additive manufacturing and sintering approaches of SiC ceramics, Open Ceramics 5 (2021) 100046, https://doi.org/10.1016/j.oceram.2020.100046.